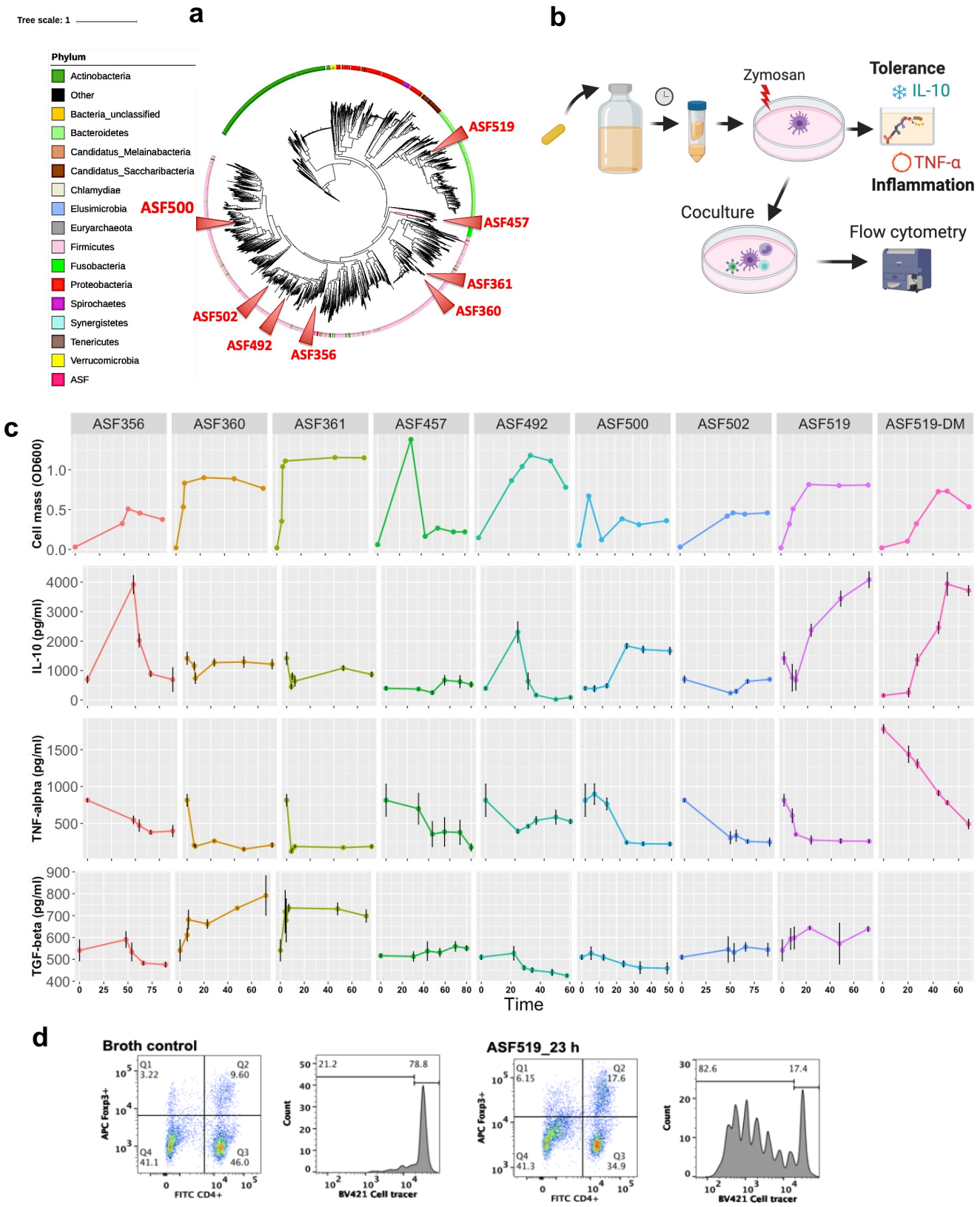

Extended Data Fig. 1 *In vitro* immunoregulatory profiles of ASF members. a, phylogeny of ASF members in the context of human gut microbiome. **b**, Experimental design to test the effect of each ASF member on representative immunophenotypes of interest. Spent media were collected longitudinally during the growth of each member, then filter sterilized for stimulation of BMDCs followed by additional exposure to zymosan (named step-wise stimulation). Cytokine levels in the supernatant of treated BMDCs were measured by ELISA kits. Treated BMDCs were co-cultured with isolated splenocytes to evaluate their impact on Treg proliferation by flow cytometry. **c**, profiles of bacterial growth and production of IL-10, TNF-a, and TGF-β by BMDCs post step-wise stimulation with spent media collected at the indicated time. All strains were cultured in BHI and ASF519 was also cultured in the defined medium (DM). All cytokine measurements have at least 3 biological replicates. **d**, Flow cytometry analysis of Treg proliferation in the coculture of cell tracer labeled splenocytes and stimulated BMDCs. Uninoculated broth control and ASF519 SSM of 23 hrs bacterial growth were used as stimuli (n=3).

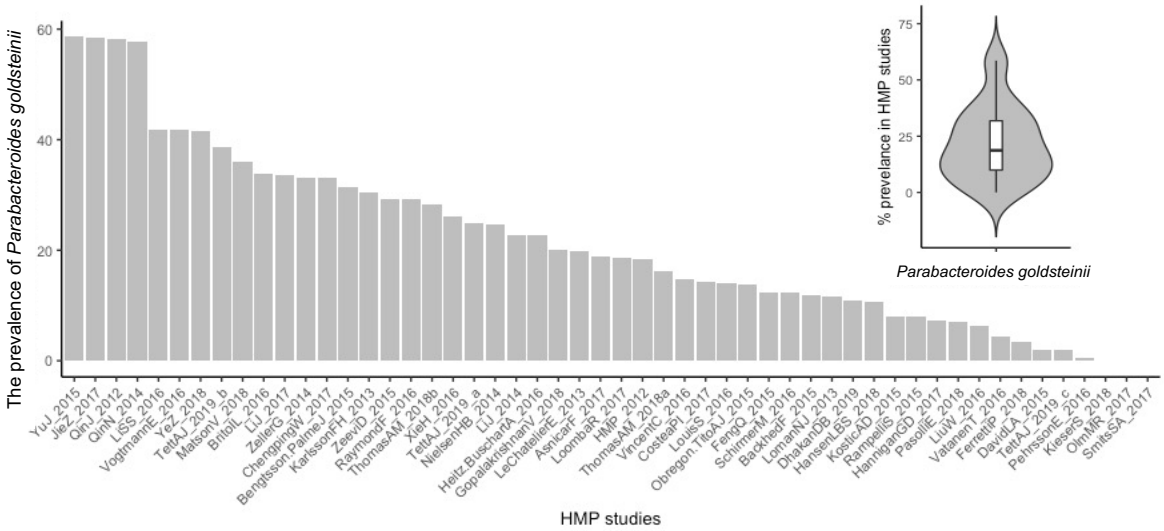

Extended Data Fig. 2 The prevalence of *Parabacteroides goldsteinii* in previous human microbiome project (HMP) studies. The inset violin plot demonstrates statistics of the prevalence data across HMP studies.

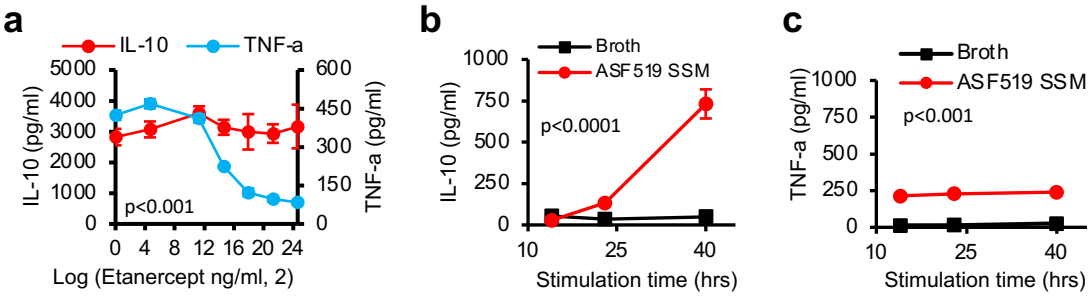

Extended Data Fig. 3 Characteristics of *Parabacteroides goldsteinii* ASF519 mediated immunoregulation. a, Effect of TNF signaling blockage on the production of IL-10 and TNF-a by step-wisely stimulated BMDCs. **b** and **c**, Effect of stimulation time on the production of IL-10 (b) and TNF-a (c) by BMDCs that were monotonously stimulated by either BHI broth or ASF519 SSM. Data are represented as mean±sd (n=3) and analyzed by two-way ANOVA. The significance indicates the difference between curves.

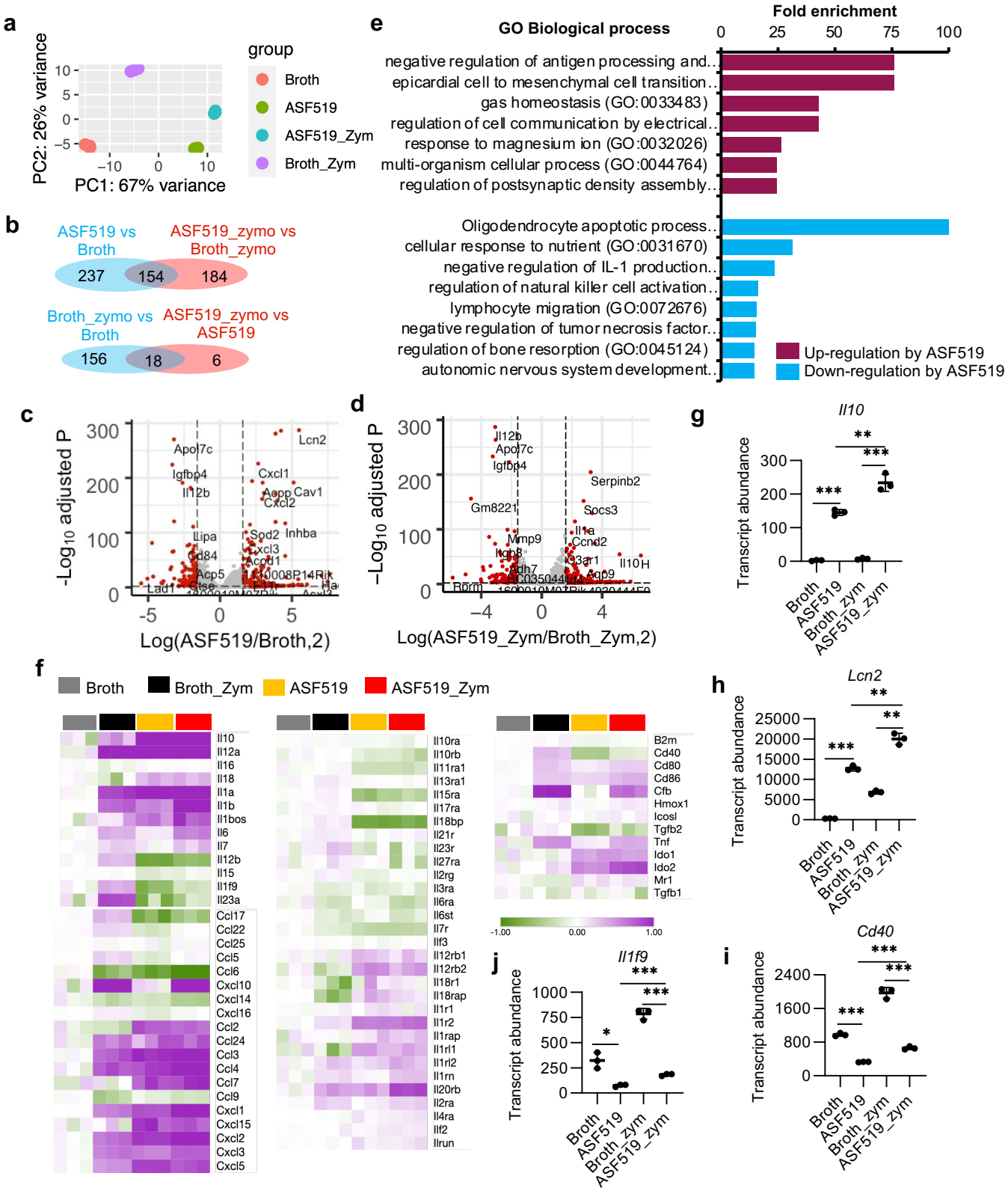

Extended Data Fig. 4 RNA sequencing data analysis of BMDCs. **a**, Principle component analysis (PCA) of normalized gene counts in samples. Each condition has 3 biological replicates. **b**, Venn diagrams showing unique and shared DEGs (p<0.01 and |fold change| >3) in different comparisons. **c** and **d**, Volcano plots for DEGs found in different conditions. DEGs are colored by red. **e**, GO enrichment analysis of upregulated and downregulated DEGs in ASF519 SSM stimulated BMDCs without further exposure to zymosan. All listed GOs are significantly enriched (adj p<0.05). **f**, heatmap plot showing the relative expression level of immune function related genes by referring to Broth. Genes encode cytokines (left), cytokine receptors (middle), complement/co-stimulatory molecules and others (right). **g-j**, plots showing a synergistic or antagonistic effect of ASF519 SSM and zymosan on the transcript abundance (n=3 per condition, mean±sd, Mann-Whitney U test, ** p<0.01, ***p<0.001).

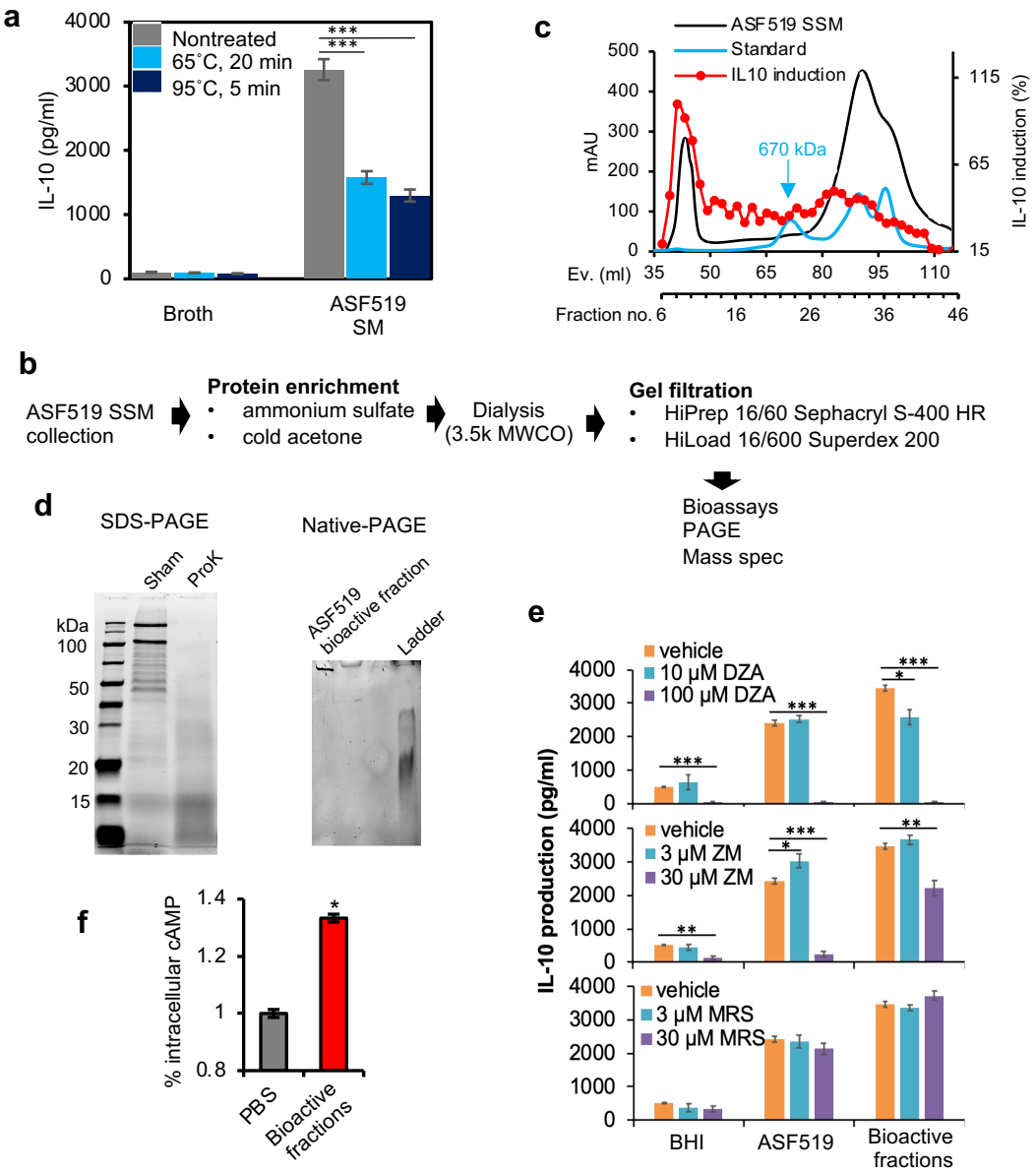

Extended Data Fig. 5 Dissecting the mechanism of ASF519 mediated IL-10 induction. **a**, Effect of heat treatment of ASF519 SSM and uninoculated broth on IL-10 induction (n=3, mean±sd, Mann-Whitney U test, ***p<0.001). **b**, Experimental workflow to identify responsible molecules. Two protein enrichment approaches (ammonium sulfate and cold acetone) have been tested to concentrate ASF519 SSM from rich BHI medium or defined medium. Two types of gel filtration columns have been applied to fractionate components for downstream analyses. **c**, IL-10 inducing function of fractions eluted from HiPrep 16/60 Sephacryl S400 HR loaded with ASF519 SSM developed from the defined medium. The UV absorbance of proteins (mAU, black) and IL-10 readouts (red) were plotted against the elution volume (Ev.) and elution fractions, colored by black and red, respectively. The gel filtration standard (blue) was run under the same condition to estimate the molecular size. The bioactive fractions were eluted in the excluded volume. **d**, PAGE analysis of bioactive fractions from gel filtration. SDS-PAGE analysis revealed degradation of ASF519 bioactive components (5 μg) by immobilized protease K (ProK) but not by 33 mM Tris-HCl (Sham). The native-PAGE analysis indicated that ASF519 bioactive components formed complex stuck in the gel well. **e**, Blockage of adenosine receptor A2a disabled IL-10 induction of BMDCs that were stimulated by BHI broth, crude ASF519 SSM, or 0.75 μg/ml bioactive fractions of gel filtration. The AHCY inhibitor 3-deazeadenosine (DZA) to block the formation of adenosine, A2a antagonist ZM 241385 (ZM), and A2b antagonist MRS-1754 (MRS), were used here. Mean±sd, n=3, Mann-Whitney U test, *p<0.05; **p<0.01; ***p<0.001. **f**, Measurement of intracellular cyclic AMP in BMDCs post step-wise stimulation. BMDCs were firstly stimulated by PBS control or bioactive fraction (0.75 μg/ml) before adding zymosan. Data are represented as mean±sd (n=2) and analyzed by two-tailed Student t test (*p<0.01).

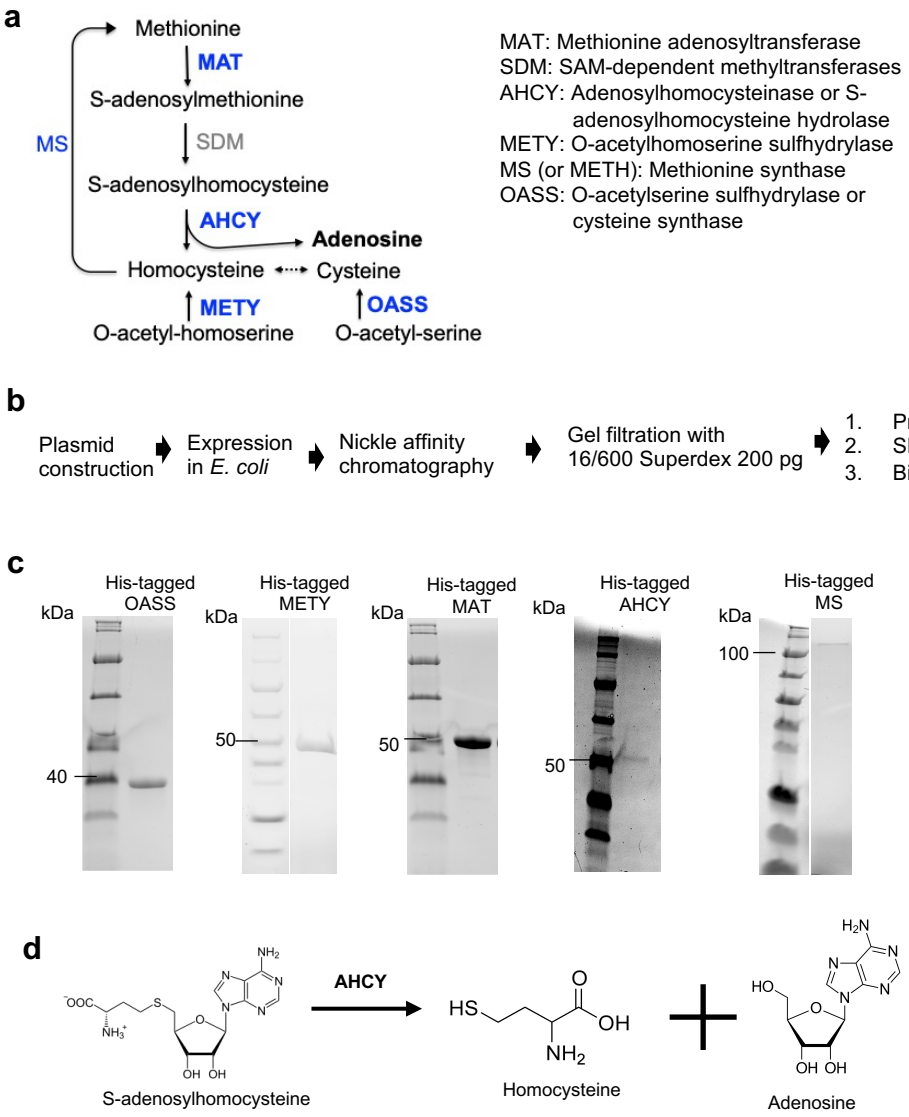

Extended Data Fig. 6 Expression and purification of His-tagged enzymes of the cysteine-methionine metabolism. a, Cysteine-methionine metabolism. The dashed line represents multiple steps of enzymatic reactions. Bold enzymes were identified in bioactive fractions of ASF519 SSM. **b**, Experimental workflow to express and purify His-tagged proteins. His-tagged proteins from the nickel affinity column were further purified with gel filtration to improve protein purity and remove endotoxin. **c**, SDS-PAGE analysis of purified His-tagged proteins, indicating high purity. **d**, Enzyme reaction of AHCY in *in vitro* assays.

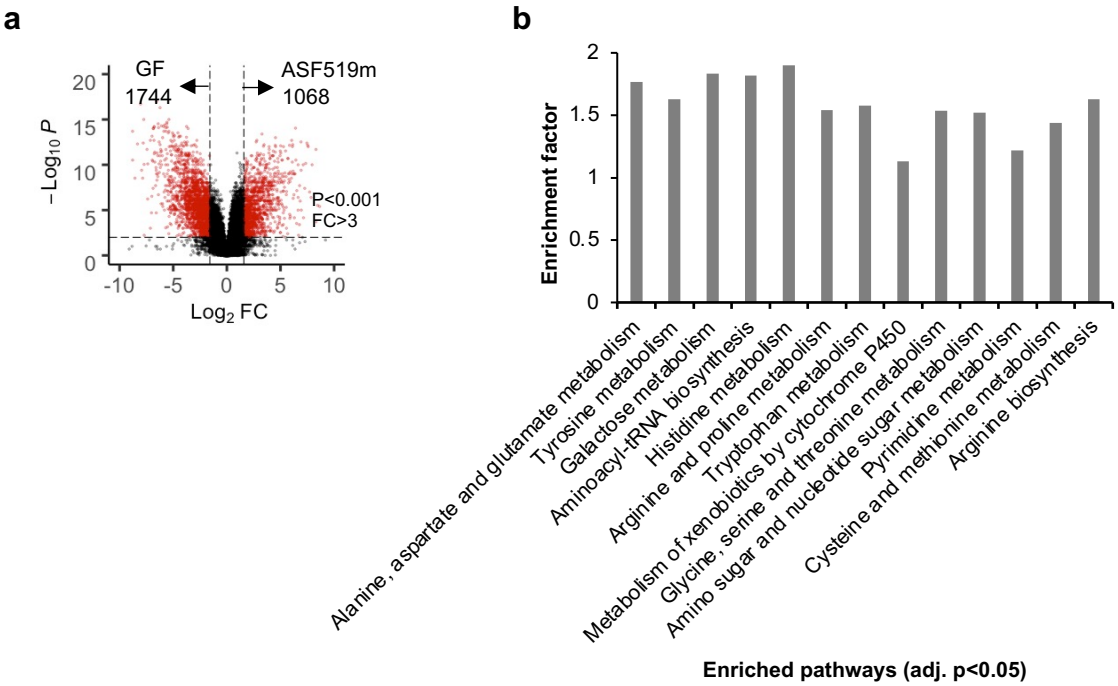

Extended Data Fig. 7 Analysis of metabolome data. a, Volcano plot showing untargeted metabolomes in cecal contents of germ-free (GF) and ASF519 mono-colonized (ASF519m) mice. Significantly changed m/z features were labeled red (adjusted P<0.001 and |fold change|>3). The signal intensity of 1068 m/z features was increased by ASF519 colonization, whereas 1744 m/z features decreased. **b**, List of metabolic pathways that were significantly influenced by ASF519 mono-association (gamma adjusted p <0.05).

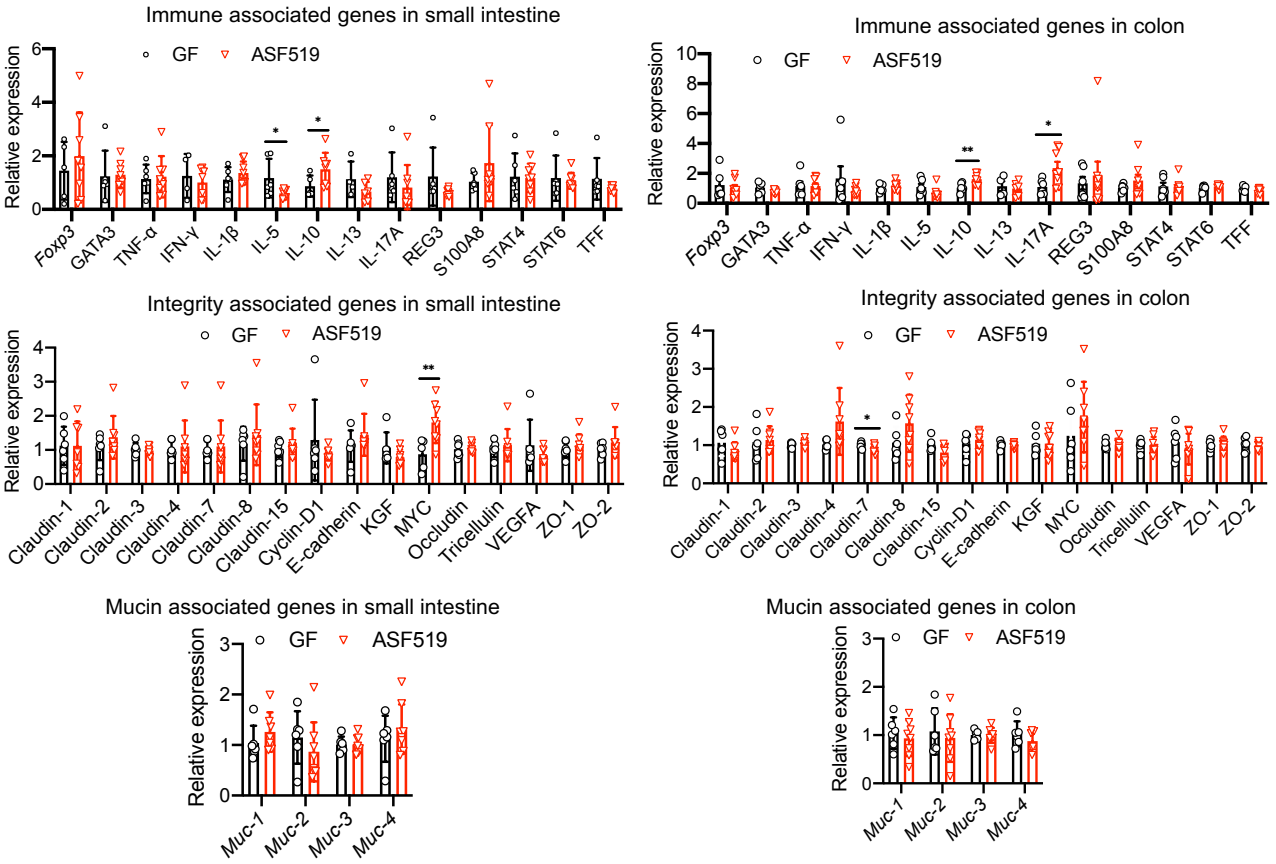

Extended Data Fig. 8 qPCR analysis to interrogate the effect of ASF519 mono-association on the transcript abundance of genes associated with immune functions, epithelial integrity, and mucin synthesis in small intestine or colon. Germ-free (GF) tissues were used. Data was normalized to the *gapdh* gene in GF tissues.

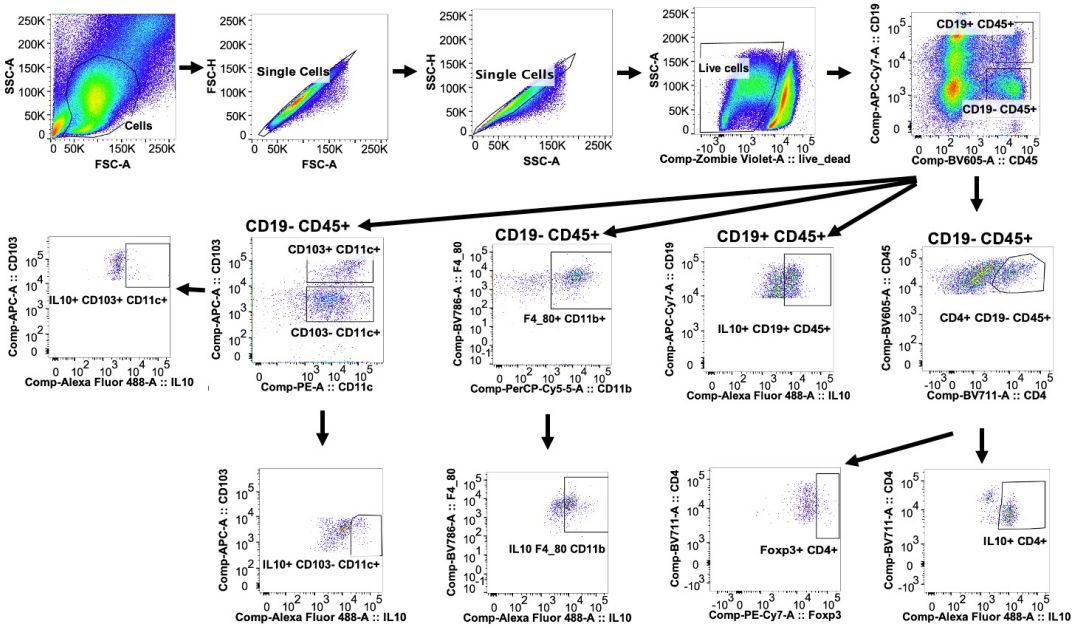

Extended Data Fig. 9 Gating strategy for flow cytometry analysis.

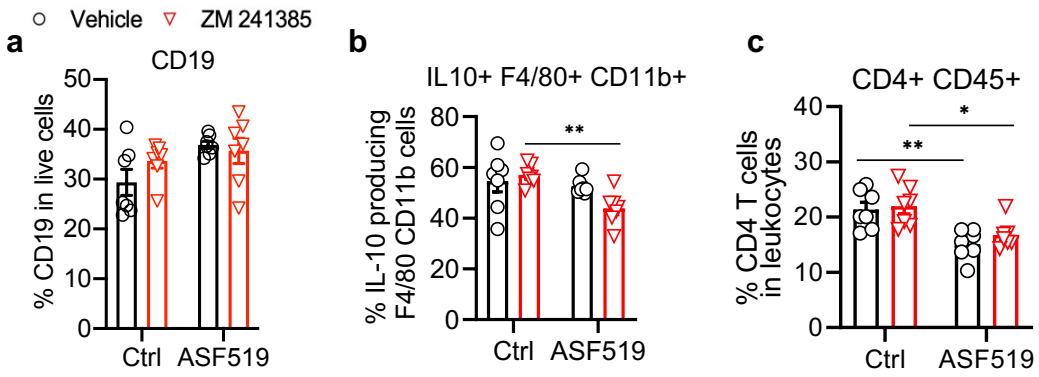

Extended Data Fig. 10 Flow cytometry analysis of cell populations in conventional mice that received killed (Ctrl) or live ASF519 and meanwhile were treated with either A2a antagonist ZM 241385 or vehicle. The population of CD19+ cells (**a**), IL-10 producing F4/80+ CD11b+ cells (**b**), and CD4+ CD45+ cells (**c**), was analyzed. Data are represented as mean±sem (n=6-8) and analyzed by two-way ANOVA along with Tukey's test (*p<0.05;**p<0.01).